Single-InN-Nanowire Nanogenerator with Upto 1 V Output Voltage

By *Chi-Te Huang, Jinhui Song, Chung-Min Tsai, Wei-Fan Lee, Der-Hsien Lien, Zhiyuan Gao, Yue Hao, Lih-Juann Chen,** and *Zhong Lin Wang**

Renewable and green energy sources would be viable candidates to meet world's energy demands.[1,2] At present, solar cells,[3–5] thermoelectric modules,[6,7] and hydrogen fuel cells[8] demonstrate possibilities of applications for future alternative energy sources. However, mechanical energy, such as wind energy, tidal energy, vibrational energy, body movements, and heart beating, also possesses the promising potential to supplement the energy needs because it exists not only almost everywhere but also at all time just in our daily life and environment. Recently, utilizing the coupling effects of semiconducting and piezoelectric properties possessed by wurtzite structured materials, such as ZnO,[9–16] ZnS,[15] CdS,[17] GaN,[18] and PVDF,[19] the piezoelectric nanogenerator has been demonstrated to convert mechanical energy into electricity. When deformed by an external force, the nanowires (NWs) would generate a piezoelectric potential (piezopotential), which acts as the driving force to propel the flowing of carriers through an external load. Moreover, the Schottky barrier between the Pt-coated AFM tip and NW serves as the gate to rectify the flowing direction of carriers.

Group III nitride materials, such as InN, GaN, and AlN are well known for their excellent optical and electronic properties.[20–23] To have superior performance and efficiency, Group III nitride nanostructures are widely utilized for the applications of electronic and optoelectronic devices, such as LEDs,[24,25] lasers,[26,27] solar cells,[28,29] and high-performance FETs.[21,22] Among Group III nitride materials, InN possesses the narrowest bandgap, the highest electron mobility, and the smallest effective electron mass.[20,30,31] Due to the unique properties, InN NWs are promising building blocks for future optoelectronic nanodevices. In this paper, the first InN NW based nanogenerator is demonstrated for harvesting mechanical energy. A detailed study is shown to present the understanding about the output generation process. Importantly, the output of a single NW can reach as high as 1 V, which is the highest among all types of NWs that have been studied. This shows its great potential for fabricating high-output nanogenerators.

The growth of InN NWs was based on a vapor-liquid-solid (V-L-S) growth process with the use Au nanoparticles as catalyst (See Experimental Section). **Figure 1a** shows a 30° tilted view scanning electron microscopy (SEM) image of the as grown InN NWs, revealing that as-synthesized samples consist of large quantity of 1D nanostructures on the surface of the Si substrate. There are high-density and uniform InN NWs with lengths up to 5 μm and diameters 25 to 100 nm. Transmission electron microscopy (TEM) analyses, including the low-magnification TEM images, high-resolution TEM (HRTEM) images, selected-area electron diffraction (SAED), and energy-dispersive X-ray spectroscopy (EDS), demonstrate the detailed crystal structures and compositions of InN NWs. The low-magnification TEM study of an InN NW shows that the NW grows along the $[01\bar{1}0]$ (Figure 1b). Figure 1c shows an HRTEM image recorded at the tip region of the InN NW shown in Figure 1b. The structure of the InN NW is found to be high-quality single crystal and free from dislocations. In addition, an Au catalyst is found to be located within the tip region of the NW and sheathed by a thin InN shell. The EDS spectra shown in Figure 1d,e are collected from the tip region and body region of the InN NW shown in Figure 1b, respectively, indicating the presence of In, N, Au, C, and Cu elements, where the C and Cu peaks result from Cu grid covered with C film.

According to our previous study, a Schottky barrier formed between the electrode and the NW plays a crucial role in the process of energy harvesting. It not only serves as a rectifier to determine the flowing direction of the carriers but also affects the efficiency and performance of piezoelectric nanogenerator.[9–15,17,18] In this study, a Schottky barrier is formed at the Pt-InN contact (see supporting information).

The schematic shown in **Figure 2a** presents the measurement system used for harvesting electricity from InN NWs. The details of the experimental setup and the measurements are the same as first utilized for demonstrating the piezoelectric nanogenerator (see supporting information).[9] The piezoelectric responses of the InN NWs are characterized utilizing an atomic force microscope (AFM) with the Pt-coated Si tip in contact mode. When the AFM tip scans across the sample, the output electrical signals, generated by deformed InN NWs, are continuously recorded across an external load (R_L).

To understand the mechanism of energy harvesting using InN NWs, the piezopotential distribution in a bent InN NW needs to be further investigated. Based on our previous study,

[*] C. T. Huang, Dr. J. H. Song, D. H. Lien, Z. Y. Gao, Prof. Z. L. Wang
School of Materials Science and Engineering
Georgia Institute of Technology
Atlanta, GA 30332 (USA)
E-mail: zhong.wang@mse.gatech.edu
C. T. Huang, C. M. Tsai, Dr. W. F. Lee, Prof. L. J. Chen
Department of Materials Science and Engineering
National Tsing Hua University
Hsinchu, Taiwan, 30013 (Taiwan)
E-mail: ljchen@mx.nthu.edu.tw
Z. Y. Gao, Prof. Y. Hao
Microelectronics Institute
Xidian University
Xi'an, 710071 (China)

DOI: 10.1002/adma.201000981

© 2010 WILEY-VCH Verlag GmbH & Co. KGaA, Weinheim
WILEY InterScience DISCOVER SOMETHING GREAT

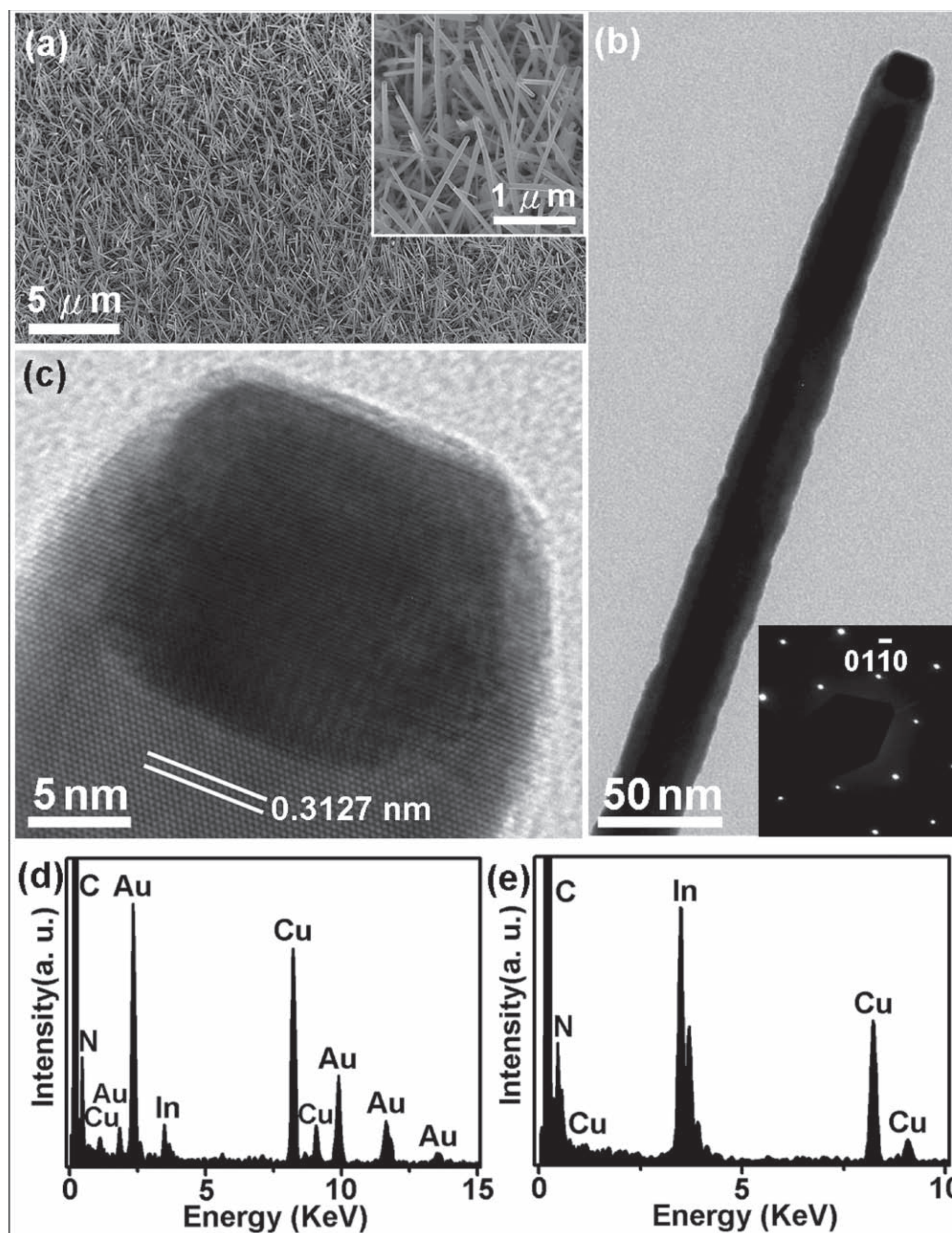

Figure 1. Crystal structures and compositions of a InN NW. a) 30° tilted view of the InN NWs. Inset is an enlarged image. b) Low-magnification TEM image of InN NW. Inset is the corresponding SAED of InN NW with [0001] zone axis. The growth direction of InN NW is along the [01$\bar{1}$0]. c) Atomic resolution TEM image of InN NW with a catalyst embedded in its tip. d,e) EDS spectra acquired from the tip region and body region of InN NW in (b).

the carrier concentration and their distribution play a significant role in dominating the magnitude of the piezopotential.[32,33] However, numerical calculation without considering the carrier concentration in a NW can give us a semi-quantitative understanding. For simplicity, the Lippman theory was utilized to calculate the piezopotential distribution in a bent InN NW.[32] The material constants of the InN NW utilized in the calculations are a = 0.3536 nm, c = 0.5709 nm, C_{11} = 223 GP, C_{12} = 115 GP, C_{13} = 92 GP, C_{33} = 224 GP, C_{44} = 48 GP,[34] piezoelectric constants $e_{15} = -0.57$ C m^{-2}, $e_{31} = -0.57$ C m^{-2}, $e_{33} = 0.97$ C m^{-2},[35] relative dielectric constants $\kappa_{11} = \kappa_{12} = \kappa_{\perp} = 13.1$, $\kappa_{33} = \kappa_{\parallel} = 14.4$,[36] and the density $\rho = 6810$ Kg m^{-3}. We assume that the InN NW grows vertically on the substrate. The tip of the NW is laterally pushed by an AFM tip with a force of 80 nN. The length and diameter of the InN NW was set to be from 1 μm to 3 μm and 50 nm, respectively. As viewed from side and in cross section, the plot shown in Figure 2b represents the calculated piezopotential distribution of a 1-μm-long InN NW with a growth direction of [0001]. The color code represents the output piezopotential. The stretched side of the InN NW would demonstrate a positive piezopotential with a magnitude of 0.191 V. The compressed side of the InN NW exhibits a negative piezopotential with a magnitude of –0.2 V. For a NW growing along [01$\bar{1}$0], the coordinate system shown in Figure 2c is defined for

© 2010 WILEY-VCH Verlag GmbH & Co. KGaA, Weinheim

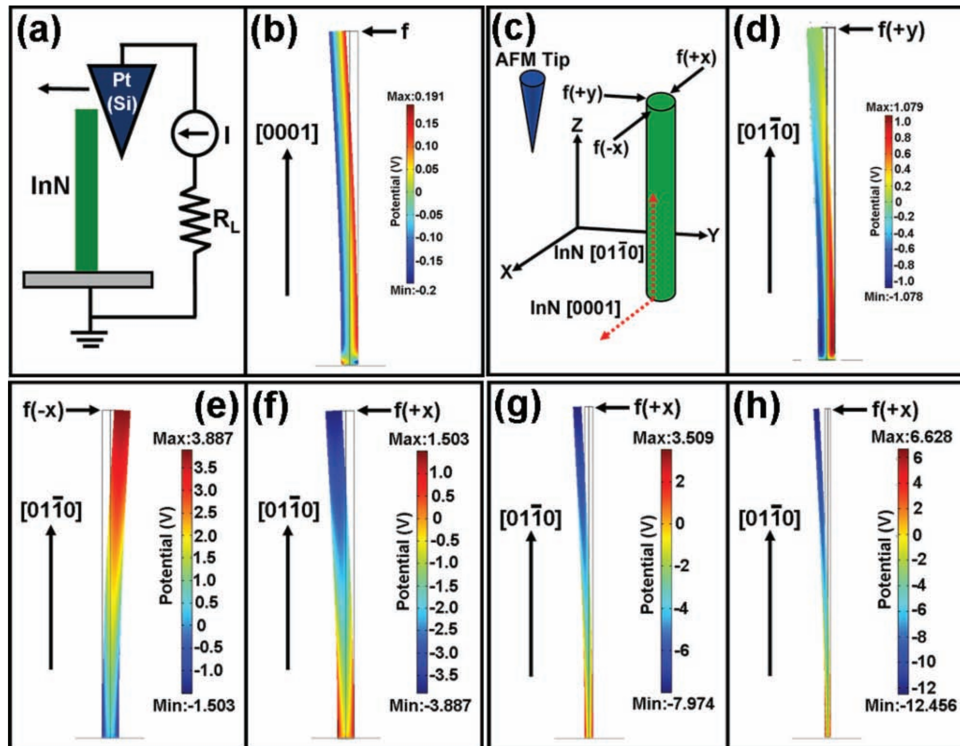

Figure 2. a) Schematic of AFM measurement system. b) Calculated piezopotential distribution at the cross section of [0001] growth InN NW with length = 1 μm and diameter = 50 nm. c) Coordinate system used to define the direction of lateral force applied from the AFM tip. d–f) Calculated piezopotential distributions at the cross section of [01$\bar{1}$0] growth InN NW under lateral force of 80 nN from three different directions. The dimensions of InN NW are length = 1 μm and diameter = 50 nm. g,h) Calculated piezopotential distributions at the cross section of [01$\bar{1}$0] growth InN NW with different length under lateral force of 80 nN. g) length = 2 μm and diameter = 50 nm. h) length = 3 μm and diameter = 50 nm.

easy description of the followiing calculation. For simplifying the calculation, we assume that the vertically aligned InN NW is laterally bent by the AFM tip through three different ways, along +y, –x, and +x axis directions. In Figure 2d, the 1-μm-long InN NW is bent laterally by the AFM tip along the +y direction. The plot reveals the stretched and compressed sides would possess positive and negative potentials, respectively. Both positive and negative piezopotential would have a maximum value at the bottom of NW. The plots of calculated piezopotential distributions in the 1-μm-long InN NW, bent by AFM tip along the –x and +x directions, are shown in Figure 2e and f, respectively. The top region of the NW would possess only positive (3.887 V) or negative (–3.887 V) potential. If we consider the influence of the carrier concentration and conductivity of n-type InN NWs on the calculation,[20,37] the magnitude of positive piezopotential would be greatly suppressed because of the screening effect of electrons. Contrary to the positive piezopotential, the negative piezopotential would be unaltered as long as the conductivity of the InN NW is not too high.[32,33] Based on the results of calculations, it was found that the magnitude and distribution of the piezopotential in a bent NW would strongly depend on the growth direction of the NW. The magnitude of negative piezopotential in the NW with a [01$\bar{1}$0] growth direction would be almost 20 times larger than that in the NW with a [0001] growth direction if the diameter, length, and applied force are the same.

When the diameter of the InN NW is kept constant at 50 nm, the influence of varying the lenght of the InN NW with growth direction of [01$\bar{1}$0] has been investigated. When the InN NW is bent by AFM tip along the +x direction, the plots of calculated piezopotential distributions shown in Figure 2g,h represent the results that the InN NW with 2 μm and 3 μm in length, respectively. The InN NW with 2 μm and 3 μm in length could generate a negative piezopotential of –7.974 V and –12.456 V, respectively. In addition, the magnitude of the positive piezopotential shown in Figure 2e depends on the length of the InN NW. The result reveals the positive and negative piezopotential generated by a bent InN NWs with 5 μm in length could reach the magnitude of about 20 and –20 V, respectively, provided that there is no doping.

The 3D electric images of output potential peaks shown in **Figure 3** are recorded continuously over the external load (R_L) when the AFM tip scans over the InN NWs with a scan area of 20 μm × 20 μm and the color code stands for the output potential. The 3D electric images shown in Figure 3a,b represent the negative and positive output signals generated by the same InN NWs, respectively. The result reveals that the InN NWs could produce not only negative output signals but also positive output signals. Almost all of the output signals are negative, and the highest output voltage could reach the value of about –1000 mV. Compared with negative output signals, only very small amount of positive output signals could be observed in

© 2010 WILEY-VCH Verlag GmbH & Co. KGaA, Weinheim

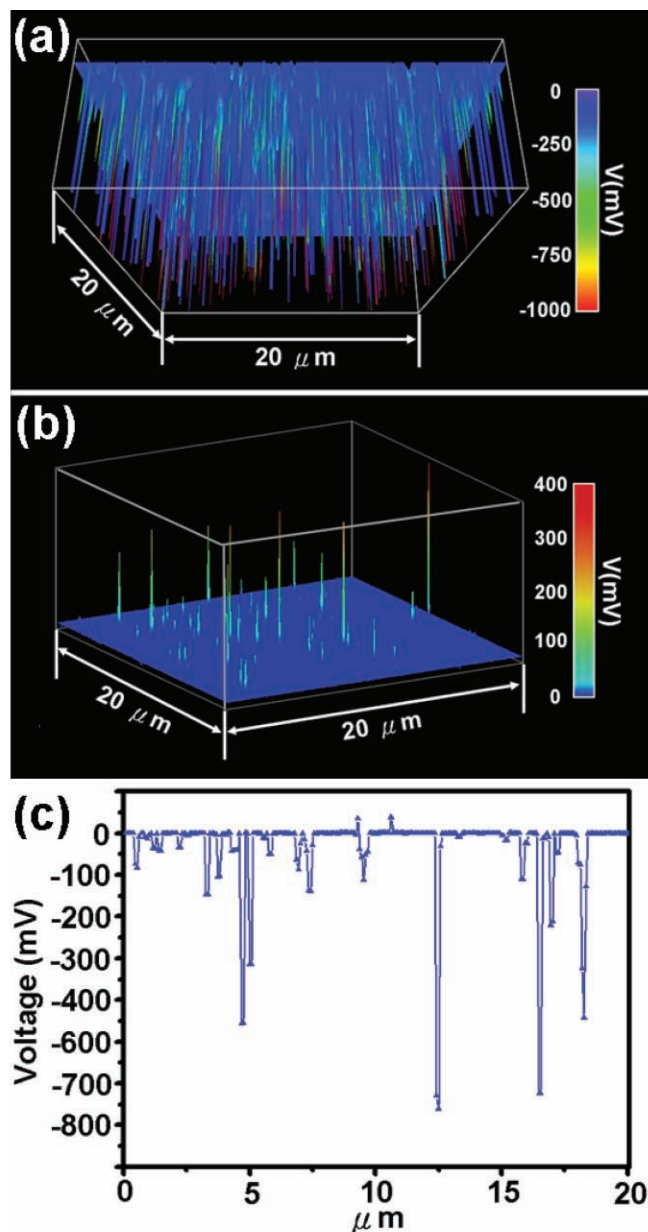

Figure 3. a) 3D Negative and b) 3D positive voltage output signals recorded across an external load when the AFM tip scanned and deflected the InN NWs with an area of 20 μm × 20 μm. c) A typical line scan profile of the output voltage, revealing the majority of output signals is negative and only small amount of positive output signals could be observed.

Figure 3b. In addition, the magnitude of output voltage is relatively small and most of them range from 0 to 50 mV. Figure 3c shows a 20 μm line profile of output signals. Almost all of the output signals are negative with the magnitude up to –800 mV. Compared with negative output signals, only small amount of relatively small positive output signals could be observed.

To understand the energy harvesting phenomena using InN NWs, the relation between the strain induced piezopotential and the Schottky barrier, formed between the Pt-coated AFM tip and the InN NW, would be the key (Figure 2). Based on the principle of the nanogenerator, the Schottky barrier formed between the Pt-coated AFM tip and the InN NW serves as a "gate" that rectifies the flowing direction of the carriers.[9–18] The Pt-coated AFM tip has a nearly zero potential ($V_m = 0$). When AFM tip is in contact with the positive piezopotential region of the bent InN NW ($Vs > 0$), it would set the Schottky diode work in the reverse biased region ($\Delta V = V_m - V_s < 0$). On the other hand, the Schottky diode would work in the forward bias region ($\Delta V = V_m - V_s > 0$) if the piezopotential generated by the bent InN NW is negative ($V_s < 0$).

Owing to the unique growth direction of the NWs, the sign and magnitude of the piezopotential in the NW depends on the direction along which the force is applied. If we consider the carriers and conductivity of the n-type InN NW,[20,37] the positive piezopotential would be greatly screened by electrons.[32,33] The case shown in Figure 2d might produce a small negative output voltage or no output voltage. The cases shown in Figure 2e,f possess a much higher piezopotential. The positive piezopotential region would be greatly screened in n-type material depending the concentration of the doping.[32,33] However there are still some positive output voltage signals appearing in the 3D electric image shown in Figure 3b. The phenomenon reveals that the screening effect does not entirely suppress the positive piezopotential, due to finite doping concentration. As a result, a small amount of the reduced positive piezopotential is large enough to overcome the reverse-biased Schottky barrier since InN exhibit a high piezopotenital according to our calculation. The high negative piezopotential shown in Figure 3a might result from the large negative piezopotential shown in Figure 2f–h, under which the Schottky diode is operated at the forward biased region. In practical experiments, once the AFM tip scans across the sample, the three cases illustrated in Figure 3d–f could happen; zero, large negative and small positive output voltage signals can be received, respectively, in agreement with our observation shown in Figure 3.

We have examined the stability and reproducibility of piezoelectric output generated by InN NWs by utilizing the same sample for all of the measurements during a period of almost 4 months. The chart shown in **Figure 4a** presents the statistical distribution of the output voltage generated by the InN NWs. The statistical result reveals that the distributions between each measurement did not change too much. About 40% to 55% of output voltages range from –1 to –20 mV and 25% to 30% of output voltages would exceed –100 mV. Most important of all, some output voltages could reach the magnitude of –1000 mV. The average number of voltage peaks and average magnitude of output voltage as a function of time are shown in Figure 4b. The average magnitude of output voltage is quite stable and is within the ranges from –110 to –120 mV. However, the average number of voltage peaks dropped a little. When the AFM tip scanned across the InN NWs, it would produce destructive damage to the InN NWs. In addition, we use the same sample for all of the measurements for almost 4 months. The drop in the average number of voltage peaks might result from the damage and wearing of InN NWs. Based on the excellent stability and performance, InN NWs would be a promising candidate for the application of piezoelectric nanogenerator.

© 2010 WILEY-VCH Verlag GmbH & Co. KGaA, Weinheim

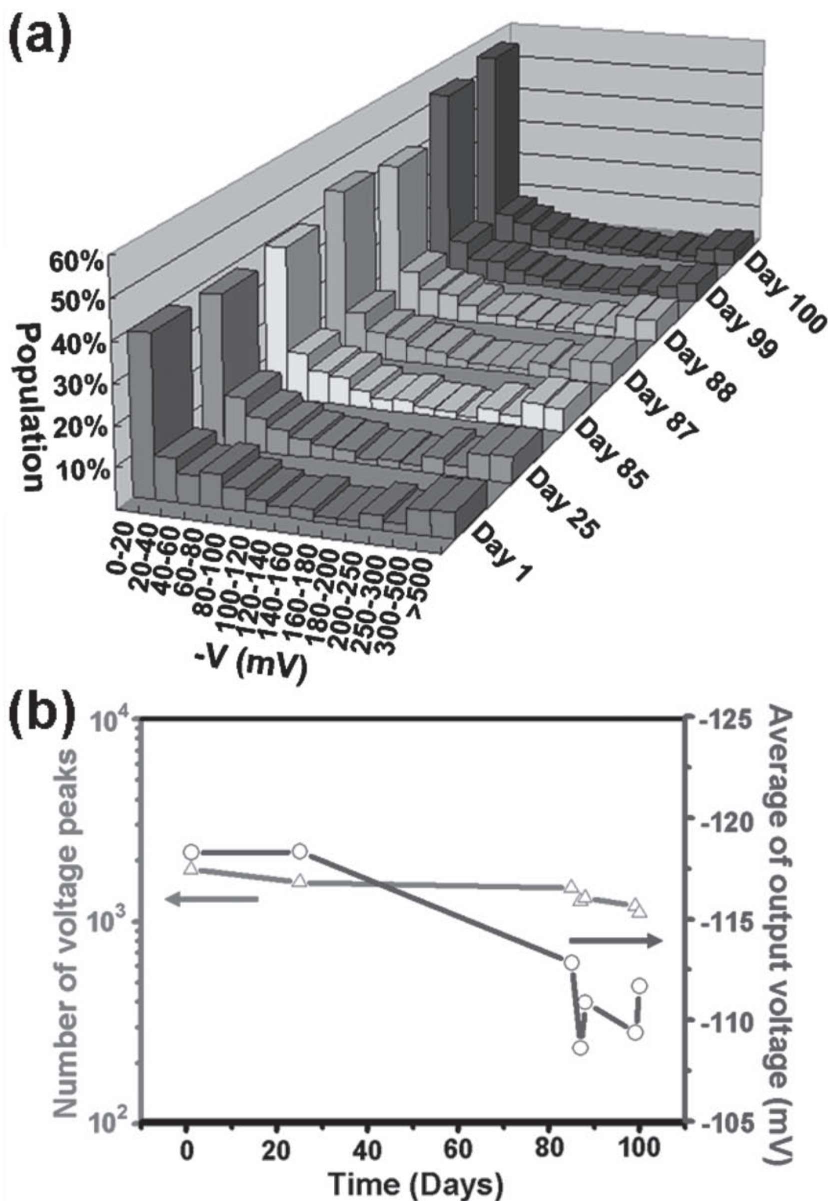

Figure 4. a) Statistical distribution of the piezoelectric output recorded from the same InN NWs sample during almost 4 months of measurements. b) The average number of voltage peaks (left axis, red triangle) and average magnitude of output voltage (right axis, blue circle) as a function of time in days for testing the reproducibility and stability of the InN NWs.

It needs to point out that the Au nanoparticle impregnated in the tip of the NW (see Figure 1) should not affect the piezoelectric measurement because a thin layer of InN around the particle is sufficient, if not all, to screen the effect of the Au tip for piezoelectric measurement.

In summary, we have successfully synthesized InN NWs via the V-L-S process. The growth direction of InN NWs is along [01$\bar{1}$0]. The calculated results reveal that the magnitude and distribution of the piezopotential in a bent NW strongly depends on the growth direction of the NW. The magnitude of the negative as well as positive piezopotential in the NW with a [01$\bar{1}$0] growth direction would be almost 20 times larger than that in the NW with a [0001] growth direction if the diameter, length, and applied force are the same. Because the positive piezopotential generated by the bent InN NW is relatively large and could not be greatly suppressed by free carriers, small amount of the reduced positive piezopotential is large enough to overcome the reverse-biased Schottky barrier. Small amount of positive output signals could be observed in 3D electric image. On the other hand, due to the high negative piezopotential generated by the bent InN NW, the InN NWs show excellent performance of piezoelectric nanogenerator. About 40% to 55% of output voltages are within the ranges from –1 to –20 mV and 25% to 30% of output voltages would exceed –100 mV. Furthermore, some output voltages could reach up to –1000 mV. The statistical result indicates that the InN NWs have excellent stability and reproducibility during almost 4 months of piezoelectric measurements. The average magnitude of output voltage ranges from –110 to –120 mV. Therefore, InN NWs show a great potential for fabricating high output nanogenerators.

Experimental Section

Synthesis of InN NWs: The growth was based on V-L-S growth process. A 2-nm-thickness Au film was deposited onto (100) Si substrates by a magnetron RF sputter system. Commercial In ingot and ammonia gas (NH_3) were used as the In and N sources, respectively. The In ingot was placed in a crucible at the center of the alumina tube. The Au-coated Si substrates were placed in the downstream region of the alumina tube for the collection and growth of InN NWs. After being evacuated to a pressure below 8×10^{-3} torr for several hours, the furnace was introduced a constant flow of 100 SCCM (SCCM denotes cubic centimeter per minute at STP) NH_3 for 60 min to reduce the concentration of the residual O_2 within the alumina tube. Then, the furnace was heated from room temperature to 900 °C at a heating rate of 20 °C min^{-1} with the NH_3 flow of 10 sccm under a pressure of 1 Torr. After reaching the desired temperature, the furnace was kept at the desired temperature for 300 min and allowed to cool down naturally to room temperature.

Supporting Information

Supporting Information is available online from Wiley InterScience or from the author.

Acknowledgements

CTH and JHS contributed equally to the research in this paper. Research was supported by DARPA (Army/AMCOM/REDSTONE AR,

© 2010 WILEY-VCH Verlag GmbH & Co. KGaA, Weinheim

COMMUNICATION

W31P4Q-08–1-0009), BES DOE (DE-FG02–07ER46394), KAUST, and NSF (DMS0706436, CMMI 0403671). Thanks are also due to National Science Council of Taiwan, Republic of China for a fellowship to study abroad (C. T. Huang). (NSC97–2917-I-007–110)

Received: March 18, 2010
Revised: April 6, 2010
Published online:

[1] Z. L. Wang, *Adv. Funct. Mater.* **2008**, *18*, 3553.
[2] M. S. Dresselhaus, I. L. Thomas, *Nature* **2001**, *414*, 332.
[3] B. Weintraub, Y. Wei, Z. L. Wang, *Angew. Chem. Int. Ed.* **2009**, *48*, 8918.
[4] W. U. Huynh, J. J. Dittmer, A. P. Alivisatos, *Science* **2002**, *295*, 2425.
[5] B. Tian, X. Zheng, T. J. Kempa, Y. Fang, N. Yu, G. Yu, J. Huang, C. M. Lieber, *Nature* **2007**, *449*, 885.
[6] A. I. Boukai, Y. Bunimovich, J. Tahir-Kheli, J. K. Yu, W. A. Goddard, J. R. Heath, *Nature* **2008**, *451*, 168.
[7] B. Poudel, Q. Hao, Y. Ma, Y. Lan, A. Minnich, B. Yu, X. Yan, D. Wang, A. Muto, D. Vashaee, X. Chen, J. Liu, M. S. Dresselhaus, G. Chen, Z. Ren, *Science* **2008**, *320*, 634.
[8] B. C. H. Steele, A. Heinzel, *Nature* **2001**, *414*, 345.
[9] Z. L. Wang, J. Song, *Science* **2006**, *312*, 242.
[10] X. Wang, J. Song, J. Liu, Z. L. Wang, *Science* **2007**, *316*, 102.
[11] R. Yang, Y. Qin, L. Dai, Z. L. Wang, *Nat. Nanotechnol.* **2009**, *4*, 34.
[12] R. Yang, Y. Qin, C. Li, G. Zhu, Z. L. Wang, *Nano Lett.* **2009**, *9*, 1201.
[13] S. Xu, Y. Wei, J. Liu, R. Yang, Z. L. Wang, *Nano Lett.* **2008**, *8*, 4027.
[14] M. P. Lu, J. Song, M. Y. Lu, M. T. Chen, Y. Gao, L. J. Chen, Z. L. Wang, *Nano Lett.* **2009**, *9*, 1223.
[15] M. Y. Lu, J. Song, M. P. Lu, C. Y. Lee, L. J. Chen, Z. L. Wang, *ACS Nano* **2009**, *3*, 357.
[16] M. Y. Choi, D. Choi, M. J. Jin, I. Kim, S. H. Kim, J. Y. Choi, S. Y. Lee, J. M. Kim, S. W. Kim, *Adv. Mater.* **2009**, *21*, 2185.
[17] Y. F. Lin, J. Song, Y. Ding, S. Y. Lu, Z. L. Wang, *Appl. Phys. Lett.* **2008**, *92*, 022105.
[18] C. T. Huang, J. H. Song, W. F. Lee, Y. Ding, Z. Y. Gao, Y. Hao, L. J. Chen, Z. L. Wang, *J. Am. Chem. Soc.* **2010**, *132*, 4766.
[19] C. Chang, V. H. Tran, J. Wang, Y. K. Fuh, L. Lin, *Nano Lett.* **2010**, *10*, 726.
[20] T. Stoica, R. J. Meijers, R. Calarco, T. Richter, E. Sutter, H. Luth, *Nano Lett.* **2006**, *6*, 1541.
[21] Y. Huang, X. Duan, Y. Cui, C. M. Lieber, *Nano Lett.* **2002**, *2*, 101.
[22] T. Kuykendall, P. Pauzauskie, S. Lee, Y. Zhang, J. Goldberger, P. Yang, *Nano Lett.* **2003**, *3*, 1063.
[23] S. K. Lim, M. Brewster, F. Qian, Y. Li, C. M. Lieber, S. Gradecak, *Nano Lett.* **2009**, *9*, 3940.
[24] Z. Zhong, F. Qian, D. Wang, C. M. Lieber, *Nano Lett.* **2003**, *3*, 343.
[25] H. M. Kim, Y. H. Cho, H. Lee, S. I. Kim, S. R. Ryu, D. Y. Kim, T. W. Kang, K. S. Chung, *Nano Lett.* **2004**, *4*, 1059.
[26] F. Qian, Y. Li, S. Gradecak, H. G. Park, Y. Dong, Y. Ding, Z. L. Wang, C. M. Lieber, *Nat. Mater.* **2008**, *7*, 701.
[27] J. C. Johnson, H. J. Choi, K. P. Knutsen, R. D. Schaller, P. Yang, R. J. Saykally, *Nat. Mater.* **2002**, *1*, 106.
[28] Y. B. Tang, Z. H. Chen, H. S. Song, C. S. Lee, H. T. Cong, H. M. Cheng, W. J. Zhang, I. Bello, S. T. Lee, *Nano Lett.* **2008**, *8*, 4191.
[29] Y. Dong, B. Tian, T. J. Kempa, C. M. Lieber, *Nano Lett.* **2009**, *9*, 2183.
[30] S. Luo, W. Zhou, Z. Zhang, L. Liu, X. Dou, J. Wang, X. Zhao, D. Liu, Y. Gao, L. Song, Y. Xiang, J. Zhou, S. Xie, *Small* **2005**, *1*, 1004.
[31] S. X. Li, K. M. Yu, J. Wu, R. E. Jones, W. Walukiewicz, J. W. Ager III, W. Shan, E. E. Haller, H. Lu, W. J. Schaff, *Phys. Rev. B* **2005**, *71*, 1612001.
[32] Y. Gao, Z. L. Wang, *Nano Lett.* **2009**, *9*, 1103.
[33] G. Mantini, Y. Gao, A. D'Amico, C. Falconi, Z. L. Wang, *Nano Res* **2009**, *2*, 624.
[34] A. F. Wright, *J. Appl. Phys.* **1997**, *82*, 2833.
[35] F. Bernardini, V. Fiorentini, D. Vanderbilt, *Phys. Rev. B* **1997**, *56*, 10024.
[36] V. Y. Davydov, V. V. Emtsev, I. N. Goncharuk, A. N. Smirnov, V. D. Petrikov, V. V. Mamutin, V. A. Vekshin, S. V. Ivanov, M. B. Smirnov, T. Inushima, *Appl. Phys. Lett.* **1999**, *75*, 3297.
[37] V. Cimalla, V. Lebedev, F. M. Morales, M. Niebelschutz, G. Ecke, R. Goldhahn, O. Ambacher, *Mat.-wiss. u. Werkstofftech.* **2006**, *37*, 924.

© 2010 WILEY-VCH Verlag GmbH & Co. KGaA, Weinheim